Monitoring Satellite Radiance Biases Using NWP Models

Roger W. Saunders, Thomas A. Blackmore, Brett Candy, Peter N. Francis, and Tim J. Hewison, *Senior Member, IEEE*

***Abstract*—Radiances measured by satellite radiometers are often subject to biases due to limitations in their radiometric calibration. In support of the Global Space-based Inter-Calibration System project, to improve the quality of calibrated radiances from atmospheric sounders and imaging radiometers, an activity is underway to compare routinely measured radiances with those simulated from operational global numerical weather prediction (NWP) fields. This paper describes the results obtained from the first three years of these comparisons. Data from the High-resolution Infrared Radiation Sounder, Spinning Enhanced Visible and Infrared Imager, Advanced Along-Track Scanning Radiometer, Advanced Microwave Sounding Unit, and Microwave Humidity Sounder radiometers, together with the Atmospheric Infrared Sounder, a spectrometer, and the Infrared Atmospheric Sounding Interferometer, an interferometer, were included in the analysis. Changes in mean biases and their standard deviations were used to investigate the temporal stability of the bias and radiometric noise of the instruments. A double difference technique can be employed to remove the effect of changes or deficiencies in the NWP model which can contribute to the biases. The variation of the biases with other variables is also investigated, such as scene temperature, scan angle, location, and time of day. Many of the instruments were shown to be stable in time, with a few exceptions, but measurements from the same instrument on different platforms are often biased with respect to each other. The limitations of the polar simultaneous nadir overpasses often used to monitor biases between polar-orbiting sensors are shown with these results due to the apparent strong dependence of some radiance biases on scene temperature.**

***Index Terms*—Calibration, numerical weather prediction (NWP) models, remote sensing, satellites.**

I. Introduction

THE operational assimilation of satellite radiances in numerical weather prediction (NWP) models provides a continuous record of the difference between the measured radiances and the equivalent simulated values computed from model fields coupled with a radiative transfer (RT) model. These differences can be due to biases in the instrument calibration or anomalies in the instrument operation which are information of value to space agencies, if available in near real time. They can also be due to the NWP models which can have consistent biases in their representation of the atmosphere/surface (e.g., water vapor concentration and surface skin temperature), but these biases do not change rapidly in time except when linked to the diurnal cycle. Also, but to a lesser extent, the RT model used to simulate the radiances may introduce a bias particularly for broad spectral channels where the fast RT model assumptions start to break down. These NWP and RT model biases should, in general, remain the same for different instruments with channels at similar wavelengths and so should cancel out when the biases between two instruments inferred from the same NWP system are differenced. It is only when interpreting the absolute value of the observed–simulated radiance biases that the model biases need to be considered. For temperature sounding channels with weighting functions which peak in the troposphere, the simulations should be accurate to better than 1 K for current state-of-the-art NWP and RT models, but for water vapor channels, the 3-D representation of water vapor in NWP models is known to have biases in some regions [1]. Before assimilation in a variational analysis which assumes unbiased Gaussian statistics, these biases have to be removed using a correction scheme [2], [3]. To calculate the effects of other gases (e.g., ozone), only climatological mean profiles are used in most NWP models, and so, large biases are to be expected in the model simulations of channels which are affected by these trace gases.

One of the objectives of the Global Space-based Inter-Calibration System (GSICS) [4] is to understand the nature of the biases seen in radiances measured by satellite instruments. These include radiometers, spectrometers, and interferometers, with the two latter sensors providing much higher spectral resolution. These biases can be due to uncertainties in the calibration of the sensor and can vary with time on orbital, daily, and seasonal timescales. The current approach of comparing the filter radiometers [e.g., the High-resolution Infrared Radiation Sounder (HIRS) and the Spinning Enhanced Visible and Infrared Imager (SEVIRI)] with high-spectral-resolution spectrometers or interferometers [e.g., the Atmospheric Infrared Sounder (AIRS) and the Infrared Atmospheric Sounding Interferometer (IASI)] for simultaneous near-nadir overpasses (SNOs) has been used with some success [5]–[7], but the area and time window available for these coincidences is very limited. Recent studies have shown [8] that the limited high-latitude SNOs from polar-orbiting satellites do not provide an adequate sampling of the instrument biases for a full range of atmospheric conditions. SNOs do, however, allow comparisons

Manuscript received February 9, 2012; revised June 15, 2012; accepted November 1, 2012. Date of publication January 21, 2013; date of current version February 21, 2013. This work was supported by the European Organisation for the Exploitation of Meteorological Satellites under several contracts.

R. W. Saunders, T. A. Blackmore, B. Candy, and P. N. Francis are with the Met Office, Exeter EX1 3PB, U.K. (e-mail: roger.saunders@metoffice.gov.uk; thomas.blackmore@metoffice.gov.uk; brett.candy@metoffice.gov.uk; pete.francis@metoffice.gov.uk).

T. J. Hewison is with the European Organisation for the Exploitation of Meteorological Satellites, 64295 Darmstadt, Germany (e-mail: tim.hewison@eumetsat.int).

Color versions of one or more of the figures in this paper are available online at http://ieeexplore.ieee.org.

Digital Object Identifier 10.1109/TGRS.2012.2229283

over a much wider range of scene temperatures than what is possible with clear-sky-only comparisons. Other studies using vicarious calibration from fixed test sites have also been made [9], but they suffer from limited sampling of the scene temperatures.

Any nonlinearities in the radiometric calibration or similar effects result in intersatellite biases which can vary with scene temperature and, hence, latitude. By comparing not only the radiances themselves but also their biases, determined by comparisons with radiances simulated from a global NWP model, more can be learned about their global nature [10], [11]. In addition, the biases computed inherently take into account differences due to spectral responses varying between common channels as the RT model calculation takes account of this. For climate applications, it has been stated [12] that an absolute calibration accuracy must be less than 0.1 K in order to be able to unambiguously determine trends. It is crucial for climate monitoring and also beneficial for NWP that we understand the characteristics of these radiance biases, and the GSICS program [13] is focused on providing some new information in this area. Before Fundamental (level 1) and Thematic (level 2) Climate Data Records are produced from the radiances, any biases must be characterized and removed.

This paper describes some results over a period of three years from November 2008 to November 2011 when the biases of a number of instruments compared with simulations from the Met Office global NWP model were analyzed. The fast RT model coupled with the Met Office unified global NWP model is described in Section II, the satellite data and processing are outlined in Section III, the methodology to compute the biases is given in Section IV, and an analysis of the results is provided in Section V followed by a summary.

II. NWP and RT Model Description

The NWP suite used for computing the simulated satellite radiances is the global version of the Unified Model (UM) at the Met Office used operationally for its weather forecasting and climate modeling applications [14], [15]. A diverse range of observations from *in situ* and satellite systems is assimilated in the 4-D variational analysis [16] used to define the initial atmospheric state for the forecast runs.

The background profile values, from a 6-h forecast off the most recent analysis, on the model grid are interpolated to the observation location and time. The model variables required for the calculation are profiles of temperature, water vapor concentration, ozone concentration, surface temperature (2 m and skin), wind speed (over ocean only), and surface pressure. Ozone, which affects some channels, is only represented by a climatological distribution [17] which is based on a reference profile (to give the vertical distribution) in the UM and then scaled by the 70-hPa temperature to give a total column amount. This scaling is based on a regression of six years of ozone retrievals with 70-hPa temperatures for each month. There is no active representation of other trace gases, which are assumed to have a fixed concentration in the RT calculations, or aerosols in the data assimilation at present. The assumed CO_2 concentration was for the year 2005. The lack of accurate ozone profile information in reality affects only one set of channels used in this study around 1039 cm^{-1} as shown in the sensitivity analysis to ozone in the right-hand column of Table I. All other effects from trace gases should be well below 0.1 K for the channels selected for this study. The only other factor will be the extinction caused by high aerosol concentrations, although, for major outbreaks, all the cloud detection schemes will identify these radiances as cloud contaminated.

The operational sea surface temperature (SST) and sea-ice analysis [18] is used to define the skin temperature over the ocean, but no allowance is made for the cooling of the skin at night ($\sim$0.15 K) or any warming due to diurnal thermoclines in the day. The model forecast profiles of temperature, humidity, ozone, and surface parameters at the observation locations are input to radiative transfer for TOVS (RTTOV) version 7, the fast RT model [19] used to compute the required radiances for the channels of interest for a specific instrument. It is important that the same version of the RT model is used throughout to ensure a consistent calculation of the simulated radiances. Broadband channels (e.g., SEVIRI 3.9-μm channel) can have biases introduced by the RT model due to the fast model assumptions breaking down. Over the ocean, the infrared (IR) surface emissivity was computed from the infrared for surface emissivity model [20] which is part of RTTOV. Over the land, an emissivity of 0.98 was used, irrespective of wavelength and location, and over sea ice, a value of 0.99 was chosen. For the microwave instruments, fast emissivity model version 2 (FASTEM-2) [21] was used to compute the emissivities over ocean, and values of 0.95 are assumed over land and first-year ice and 0.84 for multiyear ice.

Uncertainties in the surface skin temperature (and emissivity) from the NWP model can introduce significant biases in the RT simulations, but these will affect different instruments in the same way. In most cases for the surface sensing channels, only biases over the cloud-free ocean are presented here as they are expected to be small (< 0.1 K), although biases over land can also be analyzed with the data set collected.

The operational UM and data assimilation systems are periodically updated to introduce improvements. There were several changes made which could affect the radiances simulated from the model fields which are listed in Table II. The impact of some of these changes will be seen in the analysis of the biases presented hereinafter. Although the absolute bias of some channels may be affected, all instruments with similar channels will be affected in the same way.

The assimilation of satellite radiances in a variational data assimilation system requires that the radiances are unbiased with respect to the model background. As a result, the Met Office has developed a bias correction scheme based on the Harris and Kelly [2] methodology as described in [22] and [23]. This is applied to all the radiance sensors currently being assimilated at the Met Office which include advanced TIROS operational vertical sounder (ATOVS), AIRS, IASI, and SEVIRI. A suite of programs is run every model cycle (6 h) to generate observed–background clear-sky radiances (hereafter referred to as O–B), where the background radiances are radiances generated from a 6-h forecast set of profiles from the previous analysis of the UM and the observed radiances are the observed top-of-atmosphere radiances. Both the observed and background radiances are converted into equivalent

TABLE I
CHANNELS FOR WHICH O–B STATISTICS WERE COMPUTED. THE COLUMN ON THE RIGHT IS THE CHANGE IN BRIGHTNESS TEMPERATURE FOR A +10% CHANGE IN TOTAL COLUMN OZONE FOR THE IASI CHANNEL

IASI Channel	IASI cm^{-1}	AIRS Channel	AIRS cm^{-1}	HIRS Channel	SEVIRI Channel	AATSR Channel	Ozone Sensitivity
92	667.75	75	667.78	1			0.00
141	680	123	680.14	2			0.02
179	689.5	138	689.49	3			0.02
212	697.75	168	697.71				0.00
242	705.25	193	704.72	4			0.00
246	706.25	198	706.14				0.03
280	714.75	227	714.48	5			0.06
345	731	295	734.15				0.04
381	740	318	741.29				0.06
434	753.25	355	753.06	7	11		0.06
457	759	375	759.57				0.05
546	781.25	475	801.10				0.03
756	833.75	528	820.83		10	1	0.00
1121	925	787	917.31	8		2	0.00
1133	928	791	918.75		9		0.00
1579	1039.5	1088	1039.23	9	8		2.40
1991	1142.5	1260	1135.57				0.04
2019	1149.5				7		0.05
2245	1206	1263	1216.97				0.00
2741	1330	1449	1330.98	11	6		0.00
3029	1402	1583	1402.15				0.00
3339	1479.5	1681	1476.25		5		0.00
3522	1525.25	1756	1524.35	12	5		0.00
3540	1529.75			12	5		0.00
3653	1558	1794	1563.71		5		0.00
3943	1630.5				5		0.00
5130	1927.25						0.00
		1873	2188.76	13			0.00
		1897	2210.85	14			0.00
6350	2232.25	1924	2236.23	15			0.00
		1937	2248.65	16			0.00
6463	2260.5	1948	2259.26				0.00
6601	2295	1988	2298.71				0.00
6962	2385.25	2106	2385.23				0.00
6980	2389.75	2111	2390.11				0.00
6997	2394	2115	2394.03	17	4		0.00
7424	2500.75	2189	2492.08	18	4		0.00
8007	2646.5	2363	2648.75		4		0.00
		2377	2664.14	19	4	3	0.00

blackbody brightness temperature (hereafter referred to as brightness temperature) to ease their interpretation. Both uncorrected (for this study) and bias-corrected (for assimilation) radiances are computed. The routine monitoring of radiances at the Met Office is presented on the NWP Satellite Application Facility (SAF) Web site[1] for a variety of satellite sensors.

[1]http://research.metoffice.gov.uk/research/interproj/nwpsaf/monitoring.html

III. SATELLITE DATA PROCESSING

Table III lists the instruments for which data were processed as part of this study. There are a few gaps in data due to operational problems with various instruments as noted, and data collection for the Advanced Along-Track Scanning Radiometer (AATSR) only commenced in September 2010. When Meteosat-9 data dropped out, Meteosat-8 data were substituted, but the statistics were kept separate. Data from the microwave

TABLE II
TIME LINE OF CHANGES IN MET OFFICE FORECAST MODEL

Date	Model change
20 Aug 2009	Start assimilation of NOAA-19 HIRS and AMSU radiances.
10 Nov 2009	Change of model levels from 50 to 70 and model top raised from 0.1hPa to 0.01hPa.
10 Nov 2009	Change in bias correction of radiosonde relative humidity.
17 Dec 2009 to 9 Feb 2010	NOAA-17 HIRS not assimilated.
9 Mar 2010	DMSP F-16 SSMIS window channels assimilated operationally – clear scenes only over ocean.
2 Nov 2010	Modify AIRS channel selection and assumed observation errors.
2 Nov 2010	SSMIS channels 21,22 introduced to improve mesospheric/upper stratospheric analysis .
2 Nov 2010	Introduce Meteosat-9 clear sky window and water vapour channel radiances.
20 July 2011	Introduce GOES-E+W clear sky window and water vapour channel radiances.
20 July 2011	Use more IASI channels over land.
20 July 2011	Change in humidity control variable from relative humidity to normalised pseudo relative humidity [35].

TABLE III
INSTRUMENTS AND CHANNELS FOR WHICH BIAS MONITORING STATISTICS WERE COLLECTED DURING 2009–2011

Geostationary Satellite	Instrument	Channels	Source	Comments
Meteosat-8	SEVIRI	8 IR	EUMETCAST	Only when Met-9 is unavailable
Meteosat-9	SEVIRI	8 IR	EUMETCAST	
Polar-orbit Satellite	**Instrument**	**Channels**	**Source**	**Comments**
Metop-A	IASI	See Table 1	EUMETCAST	
	HIRS	9 IR	EUMETCAST	
	AMSU-A	5 MW	EUMETCAST	From Aug-10
	MHS	5 MW	EUMETCAST	From Aug-10
Aqua	AIRS	See Table 1	NESDIS	Occasional outages
NOAA-17	HIRS	9 IR	NESDIS	Gap after mid Dec-09
NOAA-19	HIRS	9 IR	NESDIS	
	AMSU-A	5 MW	NESDIS	From Aug-10
	MHS	5 MW	NESDIS	From Aug-10
ENVISAT	AATSR	3 IR Nadir 3 IR Fwd	FTP ESRIN	From 1 Sep-10. No data after 8 April 2012.

sensors were included as indicated in Table III, but the routine monitoring for these sensors did not begin until August 2010. The sources of the data are also indicated in Table III. Note that only the global data sets are included here, not the European Organisation for the Exploitation of Meteorological Satellites (EUMETSAT) rebroadcast or EUMETSAT Advanced Retransmission Service data or locally received high resolution picture transmission/high rate information transmission data.

The channels which were included in the analysis for each of the IR instruments are defined in Table I using the normal channel numbering convention for each instrument. The criterion for the selection of the IASI and AIRS channels was proximity to the HIRS and/or SEVIRI channels so that comparisons could be made between different instruments at similar wavelengths. Note that the AIRS or IASI radiances were not integrated over the HIRS-channel spectral responses as the aim was to monitor the stability of the individual channel radiances.

The Meteosat SEVIRI data set received on EUMETCAST includes all pixels, covers the full Earth disk seen by SEVIRI, and contains counts and calibration coefficients. Data during the eclipse periods are removed for slots ± 1 h from midnight to avoid spurious biases from solar radiation intrusions into the radiometer. The data set used for this study samples every fourth pixel and scan line, and a cloud detection scheme [24] is used at the Met Office for generating its clear-sky and cloud products for NWP assimilation and nowcasting applications. Very occasionally, gaps for a single slot in the SEVIRI radiance time series occur, which is thought to be due to missing data segments.

The global polar orbiter data are received from the National Oceanic and Atmospheric Administration (NOAA)/National Environmental Satellite, Data, and Information Service and EUMETSAT as calibrated radiances and processed to a common field of view by the ATOVS and Advanced Very High Resolution Radiometer (AVHRR) Pre-Processing Package (AAPP) software provided by the NWP SAF for ATOVS and IASI [25]. The radiances (which have had a correction applied to remove the mean bias) are then passed through a 1 dimensional variational analysis (1D-Var) preprocessor which allows a quality control check and a cloud cost to be computed based on a Bayesian cloud test [26] using only IR channels for IASI and HIRS and a separate cloud test for AIRS [27]. The IASI-channel subset is taken from the clearest of the four fields of view within the corresponding Metop-A Advanced Microwave Sounding Unit-A (AMSU-A) field of view. The AIRS radiances are taken from the warmest field of view within an Aqua AMSU-A field of view. One source of possible bias is due to undetected cloud in the measured radiances, and so, for this study, it is important to have very strict cloud detection criteria. As a check on the removal of cloudy pixels, histograms of the clear-sky radiances were examined and were shown to be Gaussian in shape and did not exhibit a "cold tail."

AATSR radiances are averaged values over 10-arc-minute cells, and only cloud-free data are provided in the data sets (nominally for SST retrievals) using the method described in [28]. For each averaged radiance, the number of cloud-free pixels in the grid box is also provided. Although the data are cloud cleared, experience has shown from the SST retrievals that a more rigorous cloud check is desirable. Additional cloudy flags for the cell are set if the number of clear pixels is less than 15% of the maximum possible number of pixels in the 10-arc-minute cell (nadir view) or less than 10% (forward view). This is consistent with the operational AATSR SST processing at the Met Office [29]. The maximum number of pixels in a cell is latitude dependent. An additional AATSR cloud detection O–B test is included as some pixels over uniform low stratus cloud were remaining undetected. If the $\mathbf{O}-\mathbf{B}$ value is less than -4 K for the 11- and 12-μm channels, then the data are flagged as cloudy, but this only rejected a few more pixels in persistently cloudy areas. Both the nadir- and forward-view AATSR radiances are included in the monitoring and kept separate to allow statistics for both sets to remain independent. Note that ENVISAT overpass time is in a morning orbit similar

to that of Metop-A. In late October 2010, there was a change to the ENVISAT orbit which resulted in a gap in the data stream of about a week, but the quality of the data after the maneuver appeared to be maintained. There is a climate-quality AATSR data set generated under the (A)ATSR reprocessing for climate project [30], but this is only available for historical data at present and so could not be used for this analysis.

The Advanced Microwave Sounding Unit (AMSU) and Microwave Humidity Sounder (MHS) preprocessing, in common with HIRS, uses the AAPP software [25]. The calibrated AMSU/MHS radiances are all mapped to the HIRS fields of view, and tests are applied to identify those affected by hydrometeors and complex surfaces in the microwave. A scattering index and minimizing a cost function are used to identify microwave "clear-sky" fields of view.

Only radiances which have passed the quality control checks and converged in 1D-Var are used for computing the $\mathbf{O}-\mathbf{B}$ bias. For this study, variables such as incidence angle, latitude, and longitude are all stored with each observation in the bias data sets to enable the required analysis. These data sets have been generated from November 19, 2008 (just before the Meteosat-9 SEVIRI decontamination was performed), up to December 1, 2011, for all sensors except AMSU/MHS and the AATSR instruments which started from August/September 2010. The processing is now continuing as part of the EUMETSAT NWP SAF activities. AATSR data collection ceased on April 8, 2012, when all contact with the ENVISAT satellite was lost.

IV. Methodology for Analysis

The overall technique of using NWP models to monitor radiance biases is outlined in recent papers [10], [31], where this technique is applied to AVHRR and Tropospheric Emission Spectrometer radiances, respectively. In summary, the mean bias referred to here as $\mathbf{O}-\mathbf{B}$ can be given for a channel n averaged over the region of interest for instrument j as

$$\delta B_j(n) = \frac{1}{k}\sum_{i=1}^{i=k}\left[y_n - H_n^j(x_i)\right]$$

where the number of quality-controlled clear-sky radiances y_n in the region is k and $H_n(x_i)$ is the RT model using the background model state x_i for observation i. For another instrument m with a similar channel n', we have for an observation i'

$$\delta B_m(n') = \frac{1}{k}\sum_{i'=1}^{i'=k}\left[y_{n'} - H_{n'}^m(x_{i'})\right].$$

If the center wavelengths of the channels are similar and the atmospheric absorption and surface emissivity are not changing rapidly with wavelength, we can assume that the bias from the model simulations will be the same. Assuming that they are the same, we can then do a ***double difference*** between different sensors

$$D_{j-m} = \delta B_j(n) - \delta B_m(n')$$

where D_{j-m} should be independent of any biases from the NWP and RT models and relate to the instrument biases either through errors in the calibration of the instruments or through the spectral response of the channel.

TABLE IV
Sampling of Radiances for Bias Analysis

Parameter	SEVIRI	HIRS	IASI	AIRS	ATSR	AMSU/MHS
Time	Hrly	12 hrs	12 hrs	12 hrs	12 hrs	12 hrs
Spatial	1 in 4	All	1 in 4	1 in 9	10 arc min	All
Lat	30° bands	30° bands	30° bands	30° bands	30° bands	30° bands
Long	30° bands	30° bands	30° bands	30° bands	30° bands	30° bands
Chans	8 IR	19 IR	Table 1	Table 1	Table 1	15/5 MW
Incidence angles	10° bins	10° bins	10° bins	10° bins	10° bins	10° bins
Surface type	sea/ land/ ice	sea/ land/ ice	sea/ land/ ice	sea/ land/ ice	sea	sea/ land/ ice
Cloud	Clear cloud Day/ night	Clear cloud Day/ night	Clear/cloud Day/ night	Clear/cloud Day/ night	Clear/ cloud Day/ night	Clear/ MW cloudy/ Rain
Scene radiance	10 bins	10 bins	10 bins	10 bins	10 bins	10 bins

TABLE V
Number of Observations in Millions Collected From November 19, 2008, to November 27, 2011 (AATSR Period From September 1, 2010; Microwave Instruments From August 18, 2010)

Geostationary Satellite	Instrument	Total no. Radiances X10^6	No. of clear radiances X10^6
Meteosat-9	SEVIRI	8763	2756
Polar-orbit Satellite	**Instrument**		
Metop-A	IASI	235.9	42.2
	HIRS	569.2	162.9
	AMSU/MHS	275.5	179.3
Aqua	AIRS	163.1	26.0
NOAA-17	HIRS	488.2	144.2
NOAA-19	HIRS	453.3	124.7
	AMSU/MHS	309.7	246.6
ENVISAT	AATSR	N/A	41.2

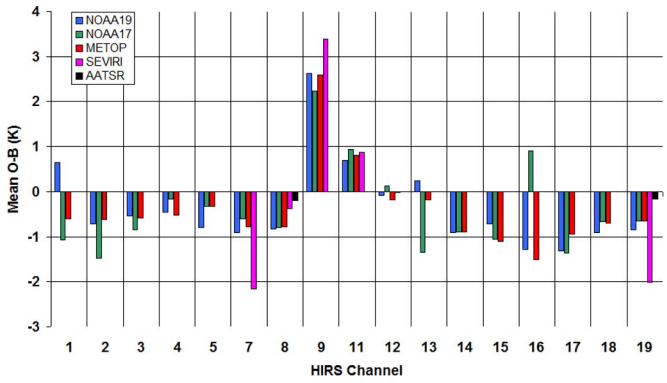

Fig. 1. Global mean O–B biases of HIRS channels over the sea for 2010. The shortwave channels are only for nighttime data. The corresponding SEVIRI- and AATSR-channel biases are also plotted for those channels which are common in wavelength.

In addition to the bias, the variance of the $\mathbf{O}-\mathbf{B}$ differences over the region of interest can also be computed. If the model background errors are stable and small enough (e.g., < 0.5 K rms for temperature profiles), this can, in some cases, be a

TABLE VI
MEAN GLOBAL O–B CLEAR-SKY BIASES OVER SEA FOR EACH OF THE HIRS INSTRUMENTS DURING 2010. CHANNELS 13–19 ARE FOR NIGHTTIME ONLY

	NOAA-17			NOAA-19			Metop-A		
HIRS	Sea	Sea	No. Obs	Sea	Sea	No. Obs	Sea	Sea	No. Obs
Chan	O-B (K)	St Dev (K)	X10^6	O-B (K)	St Dev (K)	X10^6	O-B (K)	St Dev (K)	X10^6
1	-1.08	4.40	24.5	0.65	1.68	31.1	-0.60	1.16	31.4
2	-1.47	0.70	24.5	-0.72	0.58	31.1	-0.62	0.35	31.4
3	-0.85	0.49	24.5	-0.54	0.29	31.1	-0.59	0.25	31.4
4	-0.16	0.24	24.5	-0.46	0.24	31.1	-0.52	0.25	31.4
5	-0.33	0.27	24.5	-0.80	0.30	31.1	-0.32	0.28	31.4
7	-0.60	0.52	24.5	-0.91	0.55	31.1	-0.78	0.54	31.4
8	-0.80	0.84	24.5	-0.82	0.94	31.1	-0.78	0.91	31.4
9	2.23	2.52	24.5	2.63	2.74	31.1	2.60	2.75	31.4
11	0.94	1.15	24.5	0.70	1.11	31.1	0.81	1.16	31.4
12	0.13	1.65	24.5	-0.09	1.65	31.1	-0.18	1.65	31.4
13	-1.35	0.55	11.9	0.24	0.58	13.7	-0.18	0.52	14.9
14	-0.90	0.36	11.9	-0.92	0.36	13.7	-0.90	0.37	14.9
15	-1.05	0.32	11.9	-0.72	0.33	13.7	-1.11	0.37	14.9
16	0.90	0.26	11.9	-1.28	0.39	13.7	-1.50	0.48	14.9
17	-1.37	0.67	11.9	-1.31	0.72	13.7	-0.94	0.70	14.9
18	-0.67	0.90	11.9	-0.90	1.00	13.7	-0.70	0.99	14.9
19	-0.65	0.89	11.9	-0.84	0.99	13.7	-0.65	0.98	14.9

measure of the instrument radiometric noise and any other varying effects (e.g., modulation around an orbit). To carry out a statistical analysis of the radiance biases, they are averaged over various regions defined as global, tropical ($\pm 30^\circ$ latitude), northern hemisphere ($+30^\circ$ to $+60^\circ$ latitude) and southern hemisphere (-30° to -60° latitude), and the SEVIRI area defined by the area of the Earth's disk viewed by SEVIRI up to incidence angles of 68°. Table IV lists the sampling bins in which the biases are stored for subsequent statistical analysis of their dependences on location, incidence angle, scene temperature, time of day, etc.

V. ANALYSIS OF RADIANCE BIASES

Data for the period of November 2008 to November 2011 have been analyzed to show the variation in the clear-sky $\mathbf{O-B}$ biases globally over the ocean for different sensors as a function of a number of variables. The results are summarized here.

A. Annual Global Means

The number of observations recorded for each sensor is documented in Table V. Currently, over 10^8 observations for each sensor are included in the global data sets, and so, the statistical uncertainty is negligible even after binning the data. Note that, for those shortwave channels affected by solar radiation during the day, only the nighttime data are used in the statistics here as no fast forward model for the reflected solar component was available.

The overall $\mathbf{O-B}$ statistics for 2010 for each of the IR radiometers are plotted in Fig. 1 for channels closest to the HIRS channel as defined in Table I. The global mean biases over the sea for each of the HIRS and corresponding SEVIRI and AATSR channels are plotted in Fig. 1 and also tabulated in Tables VI–VIII. The main points to note are as follows.

1) With the exception of the ozone channels (denoted channel 9), the SEVIRI 13.4-μm CO_2 channels (HIRS channel 7), and 3.9-μm window channels (HIRS channel 19), all the biases with respect to the NWP model are less than ± 1.5 K.
2) The large bias for the SEVIRI 13.4-μm CO_2 channel (HIRS channel 7) is explained hereinafter. For the 3.9-μm channel (HIRS channel 19), this is partly due to a bias from the fast RT model as the channel has a very broad spectral response compared to the corresponding HIRS channel.
3) Most of the HIRS-channel biases are similar for each instrument with the exception of channels 13 and 16 on NOAA-17 and channel 1 on NOAA-19.
4) Although not shown, the biases in 2009 were very similar to those in 2010 except for the biases of the NOAA-17 HIRS longwave stratospheric sounding channels which have progressively increased (become more negative) with time.
5) The two AATSR channels plotted show lower biases and standard deviations (Fig. 2) than the corresponding HIRS/SEVIRI channels, demonstrating the value in using this instrument as the reference and also suggesting that the HIRS and SEVIRI biases may be instrument related rather than model related or their O–B statistics are both more affected by residual cloud.

TABLE VII
METEOSAT-9 GLOBAL O–B CLEAR-SKY BIASES OVER SEA DURING 2010 FOR EACH OF THE SEVIRI IR CHANNELS. CHANNEL 4 IS FOR NIGHTTIME ONLY

SEVIRI Channel	O-B (K)	O-B St. Dev (K)	Obs X10^6
4	-2.02	0.76	232.4
5	-0.02	1.45	453.9
6	0.87	1.07	453.9
7	-0.48	0.70	453.9
8	3.39	2.70	453.9
9	-0.38	0.76	453.9
10	-0.49	0.82	453.9
11	-2.16	0.68	453.9

TABLE VIII
MEAN GLOBAL O–B CLEAR-SKY BIASES OVER THE SEA FOR THE AATSR NADIR- AND FORWARD-VIEW RADIANCES FOR THE PERIOD OF SEPTEMBER 1, 2010, TO AUGUST 31, 2011

AATSR Chan	Viewing angle	Wavelength (μm)	No. Obs X10^6	O-B (K)	St Dev (K)	Day/ Night
1	nadir	12.0	33.2	-0.479	0.649	d/n
2	nadir	11.0	33.2	-0.202	0.577	d/n
3	nadir	3.7	17.3	-0.164	0.409	n
4	forward	12.0	33.2	-0.595	0.804	d/n
5	forward	11.0	33.2	-0.266	0.710	d/n
6	forward	3.7	17.3	-0.291	0.443	n

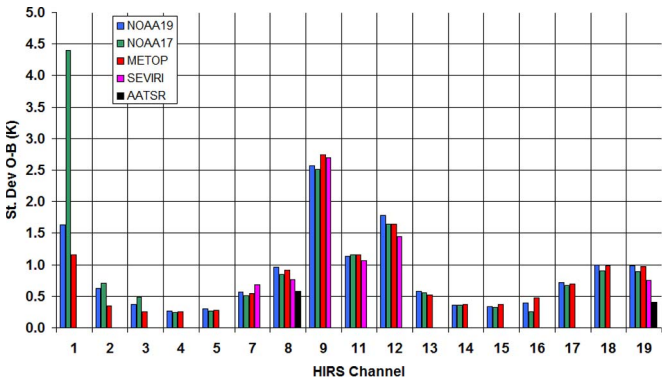

Fig. 2. Same as Fig. 1 but for the global mean standard deviation of the O–B difference for HIRS and common SEVIRI and AATSR channels.

6) The magnitude of the biases between sensors is an order of magnitude larger than the specified requirement of < 0.1 K for climate applications.

The standard deviation of the global O–B differences is plotted in Fig. 2, and here, with the exception of NOAA-17 HIRS channel 1, all instruments are in agreement, with the model error dominating for the ozone (HIRS channel 9) and water vapor channels (HIRS channels 11 and 12). The noise on the HIRS channel 1 on NOAA-17 in 2010 has increased from 2009 by 50%. This shows that the NOAA-17 HIRS detector or filter response is changing with time, making it difficult to use the longwave CO_2 channels. However, the other channels were still performing well after ten years in orbit.

AIRS and IASI radiance biases for clear sky over the ocean for the channels in Table I are plotted in Fig. 3 (bias) and Fig. 4 (standard deviation) with biases for 2009 and 2010 plotted separately. As for HIRS with a few exceptions mentioned hereinafter, all the biases are ± 1 K or less, and the biases for AIRS and IASI are similar at the same frequencies, suggesting that they are probably due to the NWP or RT model. The AIRS and IASI channels at 668 cm^{-1} have larger bias and standard deviation due to their peaking high in the stratosphere where the model error in temperature is larger. The effect of an increase in the number of NWP model levels (50 to 70 levels) is also shown with a significant reduction in the bias and standard deviation for 2010. As the channels for the two advanced IR sounders are not identical, the biases cannot be expected to be exactly the same particularly for the high-peaking channels in rapidly changing spectroscopy. The standard deviation of the IASI channels in the longwave CO_2 band (< 900 cm^{-1}) is slightly less than that of the corresponding AIRS channels except at 668 cm^{-1} where the model error dominates. In contrast, the standard deviation of the IASI channels in the shortwave CO_2 band (> 2000 cm^{-1}) is significantly higher than that of the corresponding AIRS channels. In some cases, this is due to high-peaking channels being sensitive to the larger NWP model temperature biases, and in other cases, it is due to the higher radiometric noise of IASI compared to AIRS at these wavelengths.

For the ozone channels, the bias and standard deviation are similar to those of the HIRS/SEVIRI ozone channels due to the unrepresentative ozone profile assumed in the RT model as also observed with the radiometer biases in Figs. 1 and 2.

B. Time Series

The stability of the radiometer measurements over time is important to determine for NWP, reanalysis, and climate monitoring applications. Time series plots of global mean O–B values are one way to determine the stability particularly if the double difference is employed to remove the effect of model changes.

An example of the time series of global mean O–B values for the SEVIRI 13.4-μm CO_2 channels of all the IR sensors is shown in Fig. 5 for clear-sky ocean radiances averaged over the SEVIRI full-disk area. The start of this plot is just before the SEVIRI radiometer was heated up to remove accumulated ice on the detectors in late November 2008. The sudden change in the O–B bias of $+0.7$ K after the decontamination is evident, followed by the drift in the bias during the subsequent two and a half years from -1 K to -2.9 K probably due to the buildup of water ice on the optics/detector [32]. The increase in bias is not uniform, and during certain periods, the change in bias is faster than others. This makes its use for climate monitoring, data assimilation, and cloud detection problematic unless an adaptive bias correction is used for this channel. The spectral response of the channel will also change with the ice buildup which will make the channel sensitive to a different level in the atmosphere, also potentially contributing to the bias and a height error in the peak of the Jacobian. The bias of the other HIRS 13.3-μm channels and corresponding AIRS and IASI channels also plotted in Fig. 5 shows a gradual change

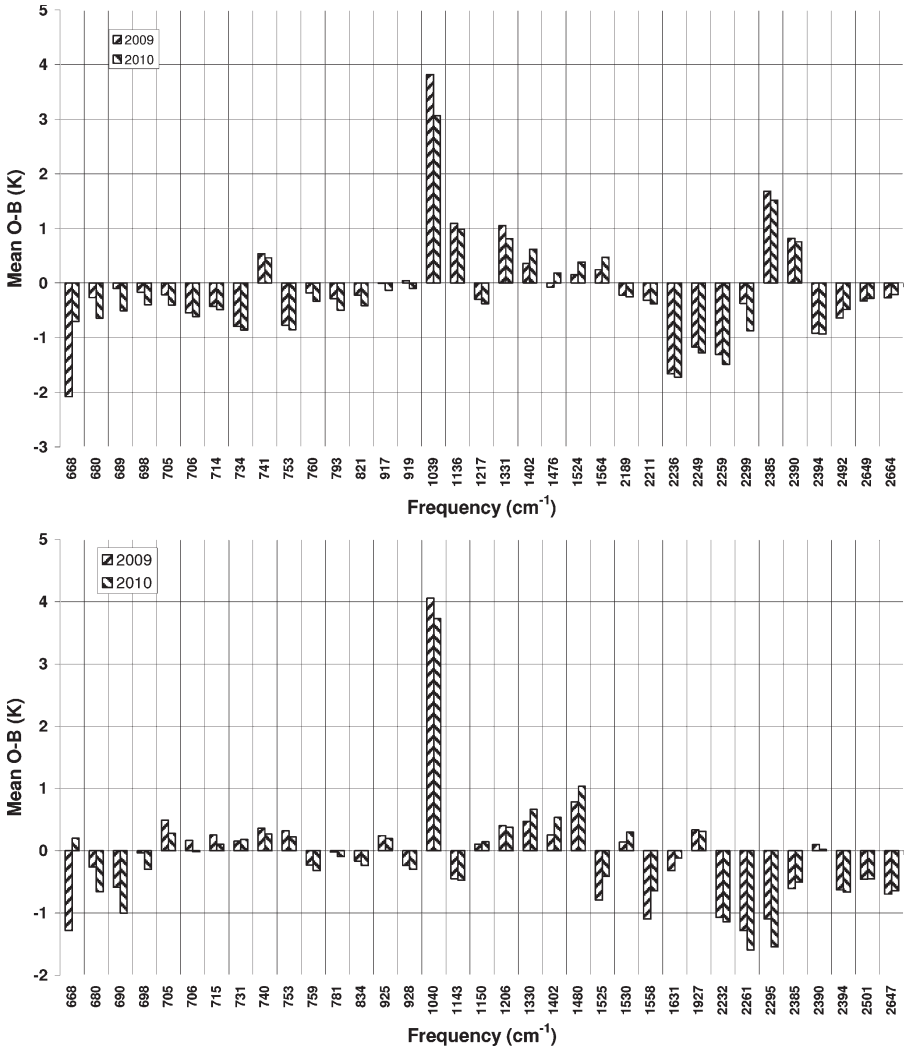

Fig. 3. (Top panel) AIRS and (bottom panel) IASI mean O–B statistics for 2009 and 2010. The shortwave channels are for nighttime only.

in the bias of about -0.3 K over three years. This is due to the assumption of a fixed CO_2 mixing ratio in the RT model, whereas in reality, the CO_2 concentration has increased by 1.5% over the period. Simulations show that, for a $+6$-ppmv increase in CO_2 (the increase from 2009 to 2011), the HIRS-channel-7 brightness temperature decreases by 0.1 K, which is less than that observed, whereas the SEVIRI-channel-11 brightness temperature decreases by only 0.08 K. It is worth noting that all the HIRS instruments have similar biases but IASI has a more positive bias which is closer to zero, and this may be due to the fact that it is more sensitive to the lower atmospheric layers than the other instruments.

Fig. 6 shows a plot for the SEVIRI 6.2-μm water vapor channel and the corresponding HIRS channel (12). Here, the biases of both channels vary significantly over the period due to changing biases in the NWP model upper tropospheric water vapor concentration, but both instruments follow each other. The double difference in the lower panel is stable between SEVIRI and HIRS. The sudden change in bias and standard deviation of all the instruments, particularly for SEVIRI and HIRS, is where the bias is reduced by 0.3 K due to the model change in the radiosonde water vapor bias correction in November 2009. Of more interest is the standard deviation of the difference where a significant decrease is seen by the HIRS and SEVIRI channels over the three years, suggesting a gradual improvement in the model's representation of upper tropospheric water vapor.

When Meteosat-9 experienced an anomaly, there were a few short periods when its radiances were replaced by those from Meteosat-8. The corresponding Meteosat-8 SEVIRI O–B biases for channel 11 (13.4 μm) had a mean difference relative to the bias of Meteosat-9 of $+1.2$ K with Meteosat-9 having the larger negative bias (not shown). This illustrates the problems when trying to derive climate data records from these instruments with the same channels but significantly different inherent biases.

The biases for the 11-μm window channels of each instrument are plotted in Fig. 7 for clear sky over ocean in the SEVIRI full-disk area. As for other channels, the HIRS biases are all very similar and quite negative (~ -0.8 K). A small negative bias is to be expected (~ -0.15 K) due to the cooling of the skin of the ocean at night. SEVIRI and IASI have very similar biases (~ -0.3 K), and AIRS has a bias much closer to zero. AATSR, only available for the last one year and three months, has a mean cool bias of -0.2 K which is close to that expected. What is also evident in Fig. 7 is a sudden change in the bias in March 2010

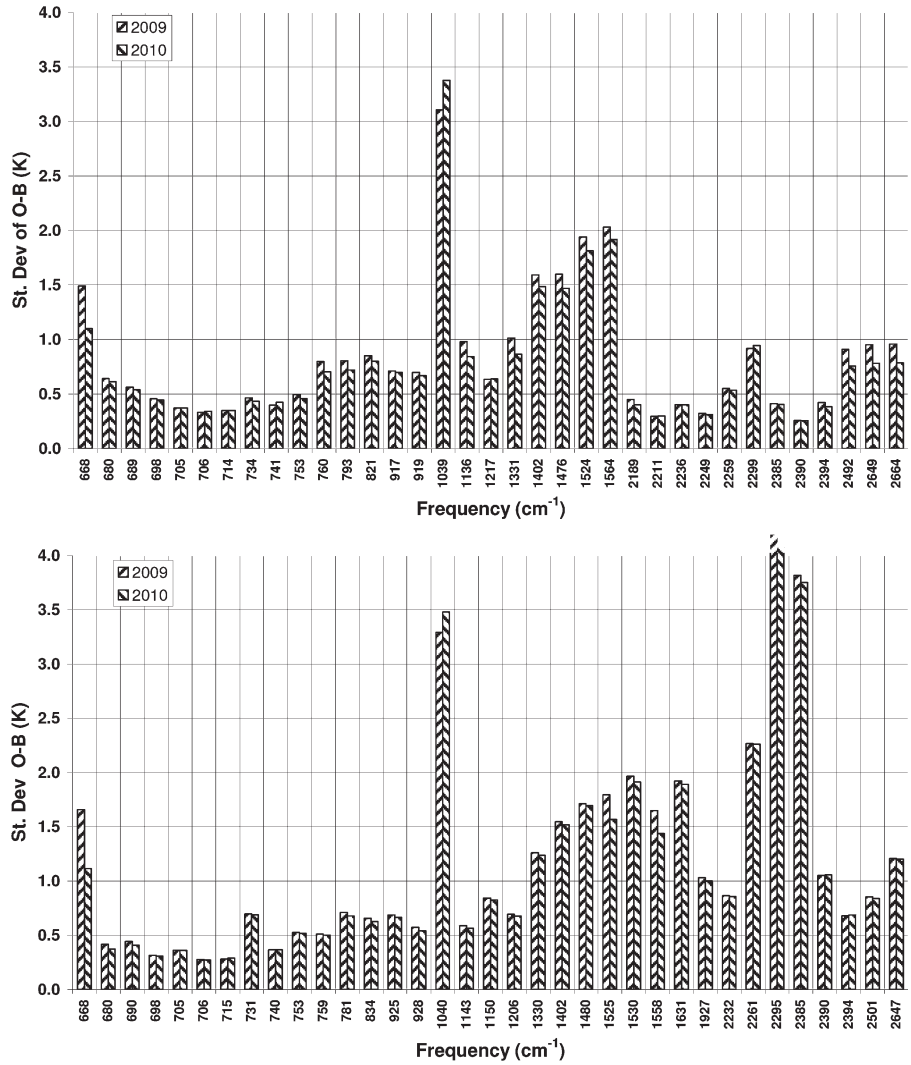

Fig. 4. (Top panel) AIRS and (bottom panel) IASI standard deviations of O–B for 2009 and 2010. The shortwave channels are for nighttime only.

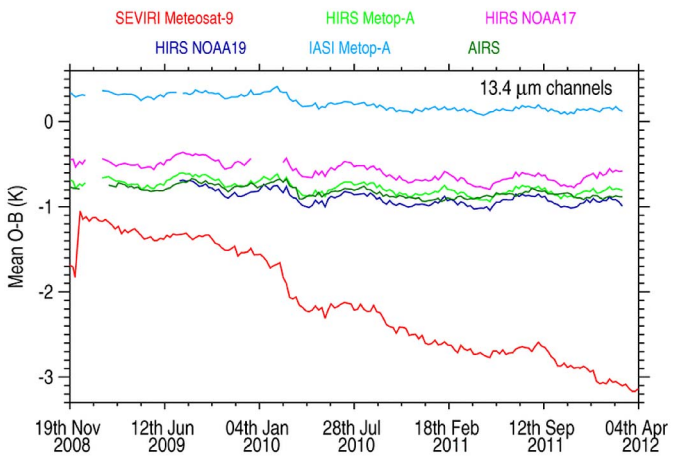

Fig. 5. Plots of the O–B mean bias for the 13-μm channels from SEVIRI (channel 11), NOAA-17, NOAA-19, and Metop-A HIRS (channel 7), AIRS (channel 355), and IASI (channel 434). All plots are just over the SEVIRI area (i.e., 60 N–60 S, 60 W–60 E) for clear-sky ocean points.

for all instruments which corresponds to the introduction of the AMSU-A and Special Sensor Microwave Imager/Sounder (SSMIS) window channels into the assimilation system which affected the low-level water vapor concentrations in the model

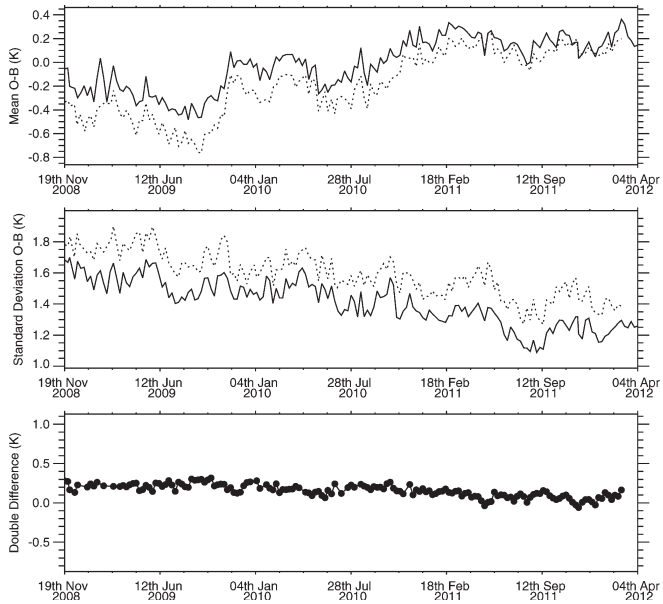

Fig. 6. Plots of 6.2-/6.7-μm channels from SEVIRI (channel 5) as solid line and Metop-A HIRS (channel 12) as dotted line. Upper panel shows the O–B global mean bias, middle panel shows the standard deviation of the difference, and lower panel shows the double difference. All plots are just over the SEVIRI area for clear-sky ocean points.

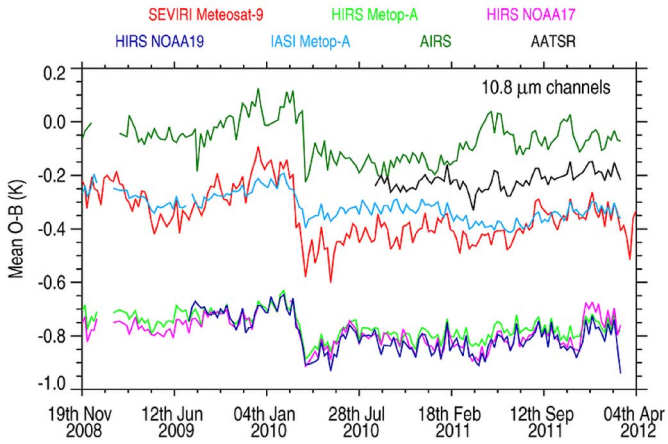

Fig. 7. Plots of the O–B mean bias for the 11-μm window channels from SEVIRI (channel 9), NOAA-17, NOAA-19, and Metop-A HIRS (channel 8), AATSR (channel 2), AIRS (channel 787), and IASI (channel 1133). All plots are just over the SEVIRI area (i.e., 60 N–60 S, 60 W–60 E) for clear-sky ocean points.

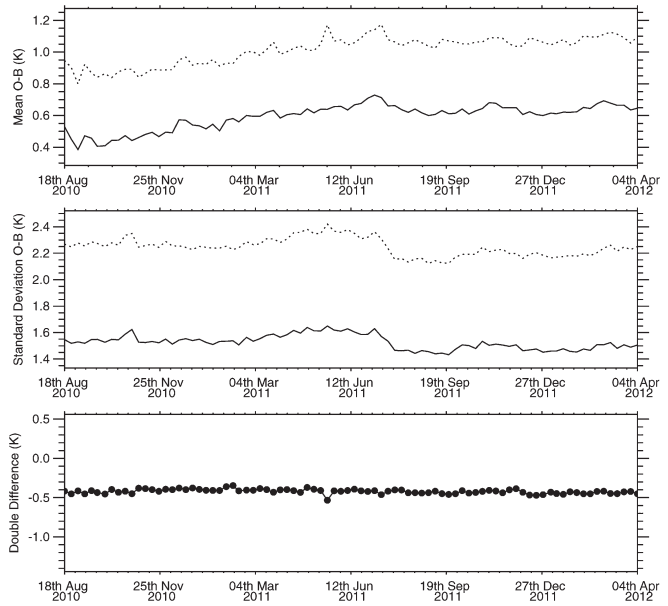

Fig. 8. Plots of MHS upper tropospheric water vapor channel (3) from (dotted) NOAA-19 and (solid) Metop-A. Upper panel shows the O–B global mean bias, middle panel shows the standard deviation of the difference, and lower panel shows the double difference. All plots are for global coverage.

and, hence, the simulated radiances for these channels. The IASI channel was less affected by this as it was a "cleaner" window channel with lower sensitivity to water vapor compared to the other instruments.

Radiance biases for the AMSU/MHS microwave channels were also collected but only for just over a year. Microwave sensors are, in general, very stable with time but can be subject to radio-frequency interference and sudden degradations in the receivers. Fig. 8 shows the mean bias and standard deviation of the difference for the high-peaking water vapor MHS channel (3) on Metop-A and NOAA-19. The biases are different for each sensor, but the double difference shows that they are stable with respect to each other. It is the same for the other lower peaking water vapor channels (not shown). The changes in bias

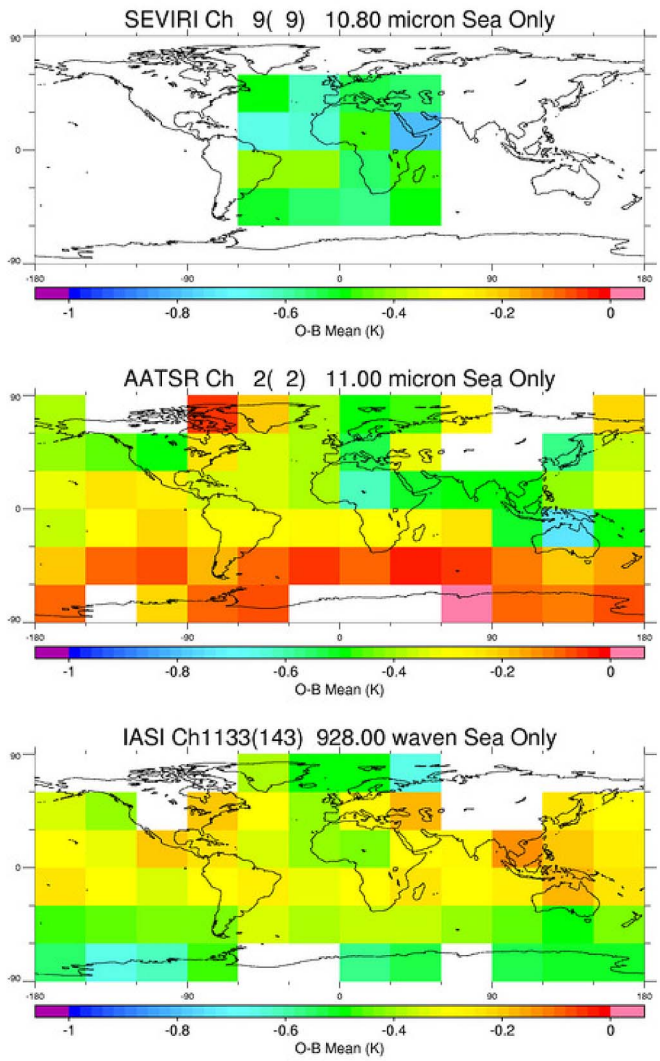

Fig. 9. Maps of SEVIRI, AATSR, and IASI clear-sky window-channel (11 μm) O–B statistics for sea points only for 2010 except AATSR which is for September 2010 to March 2011.

and standard deviation over time are similar to those seen in Fig. 6 for the IR water vapor channel which senses the same part of the atmosphere. Note that these two figures are for different areas (i.e., SEVIRI disk versus global).

C. Geographical Variations in Bias

For the polar-orbiting instruments, biases changing around an orbit are possible due to sudden changes in the instrument temperature (e.g., as the satellite crosses the terminator) or occasional intrusion of solar radiation. The biases seen with the SSMIS radiometer provide a good example of biases which vary consistently around an orbit [33].

The geographical variation of the biases of different instruments is illustrated for the 11-μm window channels in Fig. 9, which shows maps of SEVIRI, AATSR, and IASI biases for clear-sky radiances over the ocean. All the biases are negative, but whereas IASI biases are closer to zero at ~ -0.2 K to -0.4 K, SEVIRI has a bias of typically -0.4 K to -0.6 K. AATSR has a lower bias in the tropics and southern hemisphere

(< 0.3 K) than IASI but a similar bias to IASI for the extratropical northern hemisphere band. In contrast, the 6.2-μm water-vapor-channel biases (not shown) are similar for SEVIRI, HIRS, and IASI, suggesting that the bias in this case is arising from the NWP model not the instruments.

D. Scene-Dependent Bias

IR and microwave radiometers are assumed to have a linear response with incident radiation, but for a variety of reasons (i.e., detector response and use of space view as calibration reference), small nonlinearities are often present. These can be measured during instrument characterization before launch, but if not adequately taken into account, then a bias which varies with scene temperature [34] can be seen. Another possible cause, not due to the instruments, is the influence of undetected cloud for colder scene temperatures.

The observed changes in bias of the 11-μm window channels for several instruments as a function of scene temperature between 260 K and 300 K are given in Fig. 10. A limitation of our method using only clear-sky radiances is that the colder scene temperatures for high cold cloud tops are not sampled. For HIRS, the top two panels for Metop-A and NOAA-17 show a reduction in the negative bias with increasing scene temperature. SEVIRI shows a similar trend with zero bias for a scene temperature of 305 K. AIRS and IASI also show similar trends of an increasing positive bias with scene temperature which is consistent with other results [34]. It is interesting to note that AATSR shows no trend for either the nadir or the forward views, and this may be because it has two blackbodies, one at 305 K and one at 256 K. The other sensors only have one blackbody typically at 280 K and use space as the cold target. Another possible explanation is that AATSR has better cloud detection at low scene temperatures. This was investigated by comparing the AATSR nighttime-only data (where only IR channels are used for the cloud detection) with the daytime data (where visible channels are also used). The shape of the bias curve was unchanged from day to night, although the overall bias was slightly less during the day for all scene temperatures. The change in bias with scene temperature for other channels (e.g., 13.4 and 6.2 μm) exhibits a similar increase with scene temperature to that seen at 11 μm.

Another conclusion to be drawn here is that the traditional polar SNOs commonly used to compare biases from different radiometers will only sample a narrow range of cold scene temperatures and, hence, will not measure a bias representative of the global mean. It has also been demonstrated through SNOs of polar orbiters at all latitudes which become possible for short periods due to orbit drift [8].

E. Satellite Zenith Angle Dependence

It is well known that cross-track sounders have scan-dependent biases due to the changing reflective properties of the scan mirrors with incidence angle. For microwave instruments, the sidelobes in the antenna pattern also provide a contribution to the radiance which can be from parts of the spacecraft around the instrument. The first component of the bias correction

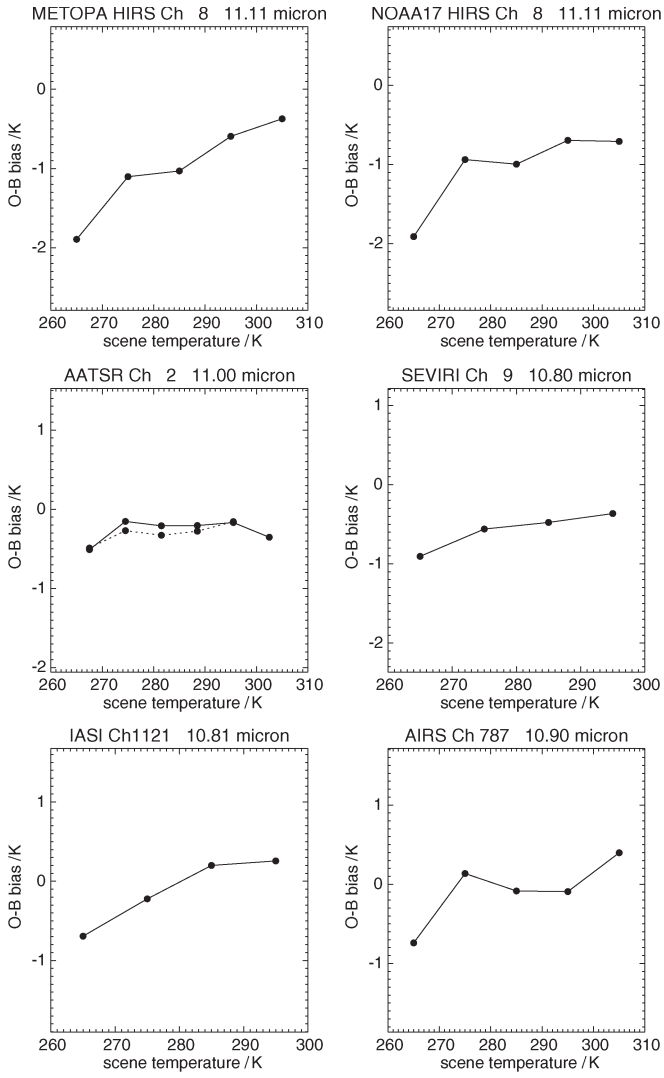

Fig. 10. Changes in O–B bias for scene temperature for the 11-μm window channels on (top panels) HIRS on Metop-A and NOAA-17, (middle panels) AATSR and SEVIRI, and (lower panels) IASI and AIRS. These are global clear-sky statistics over the ocean for 2010 except AATSR which is from September 2010 to August 2011. The dashed line on the AATSR plot is for the forward view.

schemes employed by NWP centers [2] attempts to remove this scan bias before applying a second step to remove the remaining air-mass-dependent bias. For the biases computed here, it should be borne in mind that a constant sea surface emissivity is assumed for all viewing angles in the IR simulations. For the microwave channels, the FASTEM-2 model does allow for viewing angle changes in emissivity.

Plots of the bias as a function of viewing incidence angle at the surface appear to be different for each instrument even between the cross-track sounders. For the 11-μm channels, Fig. 11 shows the cross-track variation in the biases. The HIRS-channel-8 biases for three different satellites show a very similar behavior with symmetrically increasing biases away from the nadir view with magnitudes of 0.3 K from nadir to the edge of the scan. IASI also exhibits a similar behavior but with half the magnitude and in the opposite sense (lower biases at the swath edge), suggesting that the properties of the HIRS scan mirrors introduce a scan-dependent calibration

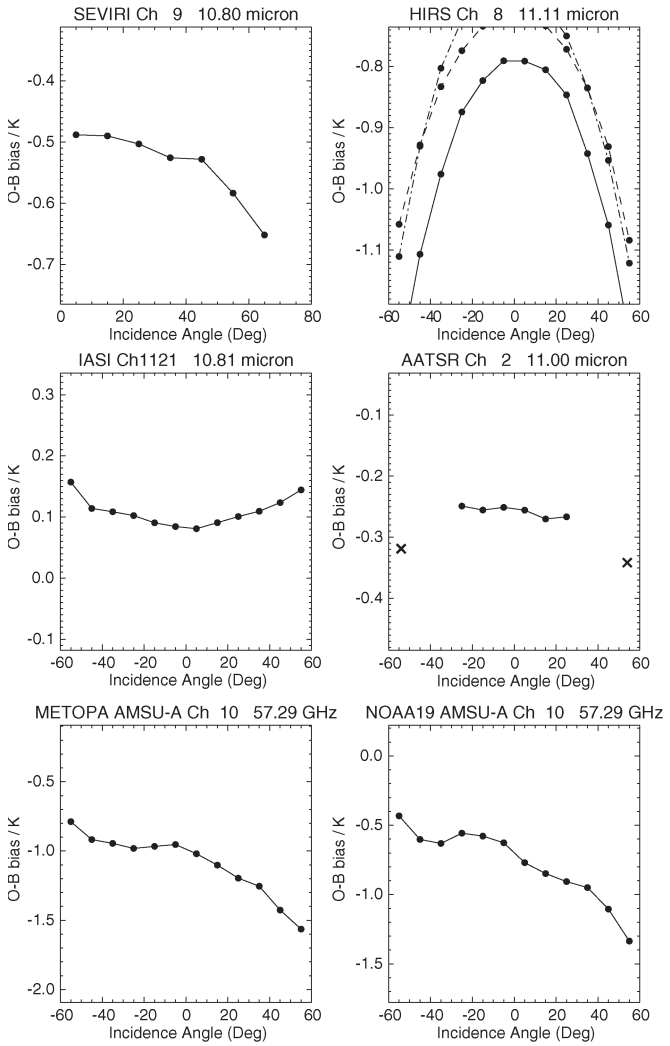

Fig. 11. Plots of the mean clear-sky bias for the 11-μm channels of SEVIRI, HIRS, IASI, AATSR, and ASMU-A as a function of incidence angle at the surface. The three lines on the HIRS plot correspond to data from Metop-A, NOAA-17, and NOAA-19. The crosses on the AATSR plot correspond to the forward view. The data are over the ocean for 2010 except AATSR which is from September 2010 to August 2011.

error. Although the SEVIRI imaging radiometer has a different viewing configuration, the dependence on incidence angle is the same as that for HIRS. AATSR with an offset conical scan of the surface shows no consistent changes in bias over its limited scan angle range for the nadir view, but the forward-view bias is 0.08 K larger. The fact that the changes in HIRS and IASI scan biases are of opposite sign suggests that the impact of the fixed model emissivity on the results is negligible. AIRS biases (not shown) are slightly larger than those for IASI but are much smaller than those for HIRS with a 0.2-K change from nadir to the edge of the scan.

The biases for the 13.4-μm channels on each instrument at the edge of their scans are at least 0.1 K different from the nadir-view biases (not shown). SEVIRI, with a different scan geometry, has a stronger dependence with an increasing negative bias up to -2.8 K with higher zenith angles up to 45°, and then, the bias reduces for large angles. These large scan angle dependences in sounding channels suggest that at least part of the apparent bias is due not only to radiometric

TABLE IX
DAY–NIGHT RADIANCE DIFFERENCES IN KELVINS FOR IR WINDOW ($\sim$10.8 μm), CO_2 ($\sim$13.4 μm), AND UPPER TROPOSPHERIC HUMIDITY ($\sim$6.5 μm) CHANNELS. THE DATA ARE OVER CLEAR-SKY OCEAN FOR THE PERIOD OF SEPTEMBER 1, 2010, TO AUGUST 31, 2011, AND ARE RESTRICTED TO THE REGION 60° N–60° S, 60° W–60° E

Instrument and (channel number)	Overpass time (UTC)	10.8 micron channel	13.4 micron channel	6.5 micron channel
SEVIRI (9, 11, 5)	Hourly	0.30 K	0.14 K	0.03 K
HIRS NOAA-19 (8,7,12)	14:00	0.25 K	0.08 K	-0.02 K
HIRS NOAA-17 (8,7,12)	11:00	0.03K	0.03K	0.09 K
HIRS Metop (8,7,12)	10:00	0.08 K	0.04 K	0.11 K
IASI (1133, 434, 3522)	10:00	0.04 K	0.05 K	0.02 K
AIRS (787, 355, 1756)	13:30	0.12 K	0.04 K	-0.03 K
AATSR (2)	10:15	0.14 K	N/A	N/A

calibration errors but also to errors in their assumed spectral response functions, which can modify the channels' weighting functions and, hence, their variation with scan angle.

The scan angle dependence of the AMSU-A temperature sounding channels is also significant as illustrated in the lower panels of Fig. 11 for Metop-A and NOAA-19 AMSU-A channel 10. This has also been reported in [9]. This bias was found to be consistent between instruments and is stable with time, allowing a fixed bias correction to be effective for assimilation. It is surprising that the bias is not more symmetric about nadir for this channel, but the radiometer "sees" parts of the instrument and spacecraft in its sidelobes which can cause this asymmetry. Other AMSU-A channels show a similar behavior, although surface sensing channels are more symmetric.

F. Day–Night Differences

The change in bias between daytime and nighttime has also been investigated. For SEVIRI, the full diurnal cycle can be sampled, but for the polar orbiters, only one daytime and nighttime measurement is taken at one location; thus, the day minus night difference will strongly depend on the local overpass times. For the platforms included here, NOAA-19 and Aqua have early afternoon overpasses and so would be expected to have the biggest diurnal changes. This is clearly illustrated in Table IX, where the day–night bias differences over the ocean in the SEVIRI coverage area are given. The SEVIRI data are averaged over all the daylight hours, whereas the polar data are just representative of their overpass times.

As expected, the Metop-A and NOAA-17 instruments show smaller diurnal changes. The reason for the diurnal changes is probably originating in the model which does not represent the diurnal thermocline in the sea surface skin temperature, and this potentially can introduce localized biases of several

kelvins. Maps of the day–night differences for SEVIRI and NOAA-19 HIRS (not shown) are similar for both instruments, suggesting that the differences do originate from the model. The AATSR day–night difference in Table IX appears to be anomalously high relative to that of the Metop instruments, and it is most likely due to the fact that it has a more effective cloud detection during the day using the visible-channel radiances which increase the detection of low uniform cloud, making daytime radiances slightly warmer. The other instruments (except SEVIRI) have the same cloud detection during the day and night.

For the 13.4-μm temperature sounding channels, there is still evidence of a smaller diurnal variation for SEVIRI, as shown in Table IX, and perhaps HIRS on NOAA-19, but IASI and AIRS show no significant day–night difference. The 6.5-μm water vapor channels on SEVIRI and all the polar sensors show no significant evidence of a day–night difference as they are insensitive to the surface.

VI. Summary and Discussion

This study has, for the first time, compiled a comprehensive data set of the measured radiances from several different satellite instruments and compared them with the corresponding radiances simulated from a state-of-the-art NWP 6-h forecast field. The radiance biases computed are binned according to various different criteria to allow an analysis of the behavior of these biases for several different parameters (e.g., time, location, scene temperature, and incidence angle). The main conclusions from this analysis of the data are summarized here.

Changes in the NWP system can introduce changes in the bias as observed in November 2009 when the model upper tropospheric humidity characteristics were changed which affected the water vapor channels. However, by using the double difference technique between different satellite sensors, the impact of the model changes can be largely removed.

The trend in the drift of the radiance of the SEVIRI 13.4-μm channel using SNOs with other sensors [32] is confirmed using NWP O–B bias statistics presented here. This is caused by the buildup of ice on the detector for this channel. The change in bias is not linear with time but has sudden increases periodically. By autumn of 2011, the relative bias had reached -2.9 K which is averaged over all clear scene temperatures. The GSICS bias monitoring of this channel with respect to IASI suggests a bias of -1.8 K, but this is for a normalized "standard scene temperature" and so cannot easily be compared to the biases presented here. All other SEVIRI channels appear to be stable over the period of this analysis (2009–2011) except for the ozone channel which could not be simulated by the NWP model accurately enough to provide a reliable estimate of the bias.

Comparisons between SEVIRI and HIRS channels were more consistent than those between SEVIRI and IASI or AIRS because the spectral coverage of HIRS and SEVIRI are more similar, which leads to a similar depth of atmospheric layer being sampled. For strict comparisons, this shows the need to integrate the IASI or AIRS radiances over the SEVIRI-channel spectral responses. The O–B biases of the 13.4-μm channels on SEVIRI, IASI, and HIRS (on Metop-A) are all significantly different from each other, highlighting the differences between instruments and the need for bias correction. The O–B bias for the SEVIRI 13.4-μm channel on Meteosat-9 is 1.2 K larger than that for the same channel on Meteosat-8. This inconsistency between the same instruments on different platforms is a concern for climate monitoring purposes and highlights the need for their intercalibration. In contrast, for the 6.2-μm water vapor channel, the biases are all of similar magnitude, which, in this case, is due to the biases in the NWP model water vapor distribution dominating.

The behaviors of all three HIRS sensors on Metop-A, NOAA-17, and NOAA-19 are similar, but the NOAA-17 HIRS channel 1 has an increasing standard deviation in the O–B values between 2009 and 2011, suggesting a degradation in the instrument over time.

The variation of the bias with several different parameters has also been investigated. In general, the O–B bias becomes more positive with increasing scene temperature for all instruments except AATSR where the bias was found to be independent of scene temperature. This is interesting because the AATSR is the only sensor which has two blackbodies, one at 260 K and one at 280 K. The other sensors all use space as the cold target, and so, this result should be investigated further to see if it could have implications for the design of future radiometers for climate monitoring. The change in bias from one edge of the swath to the other (i.e., a function of scan angle) is not insignificant from a climate perspective at about 0.1 K for AATSR and IASI, 0.2 K for AIRS, and 0.5 K for HIRS. For SEVIRI, there appears to be a gradual increase in the negative bias away from nadir for the 10.8-μm window channel but a minimum in the bias at 45° for the 13.4-μm and other sounding channels. For the AMSU microwave radiances, there is a strong scan angle dependence which is not symmetrical about nadir but is the same for NOAA-19 and Metop-A and stable in time. The stability of the AMSU microwave radiances with time has been demonstrated, although the same channels on different satellites can have quite different biases.

A day–night difference in the O–B bias is observed for clear-sky surface sensing channels, probably due to the diurnal thermocline over the ocean not being represented in the model and also differences in the cloud detection. It is not evident for the upper tropospheric channels.

These results have shown that O–B biases from the Met Office global NWP system can be used as a powerful tool to monitor radiances from all instruments and to intercompare them. This data set of several years will start to inform the utility of these measurements for climate trend monitoring and exploitation in reanalyses (e.g., European Reanalysis of Global Climate Observations). It is planned to continue this work within the EUMETSAT NWP SAF activities and obtain longer time series to understand better the bias characteristics of each instrument for generation of climate data sets. Other instruments (e.g., Advanced Technology Microwave Sounder and Cross track Infrared Sounder on Suomi-NPOESS Preparatory Program) may also be included in the data collection and analysis in the future. Finally, it would be interesting to compare the biases reported here with the Met Office model with those seen at other NWP centers to help separate out the model biases from the instrument biases.

ACKNOWLEDGMENT

The satellite data were provided by the European Organisation for the Exploitation of Meteorological Satellites, European Space Agency, and National Oceanic and Atmospheric Administration as part of the real-time delivery of data to the Met Office for its operations.

REFERENCES

[1] S. M. Newman, R. O. Knuteson, D. K. Zhou, A. M. Larar, W. L. Smith, and J. P. Taylor, "Radiative transfer validation study from the European Aqua Thermodynamic Experiment," *Q. J. R. Meteorol. Soc.*, vol. 135, no. 639, pp. 277–290, Jan. 2009.

[2] B. Harris and G. Kelly, "A satellite radiance bias correction for data assimilation," *Q. J. R. Meteorol. Soc.*, vol. 127, pp. 1453–1468, 2001.

[3] D. P. Dee and S. Uppala, "Variational bias correction of satellite radiance data in the ERA-Interim reanalysis," *Q. J. R. Meteorol. Soc.*, vol. 135, no. 644, pp. 1830–1841, Oct. 2009.

[4] M. Goldberg, G. Ohring, J. Butler, C. Cao, R. Datla, D. Doelling, V. Gaertner, T. Hewison, B. Iacovazzi, D. Kim, T. Kurino, J. Lafeuille, P. Minnis, D. Renaut, J. Schmetz, D. Tobin, L. Wang, F. Weng, X. Wu, F. Yu, P. Zhang, and T. Zhu, "The Global Space-based Inter-Calibration System (GSICS)," *Bull. Amer. Meteorol. Soc.*, vol. 92, pp. 467–475, 2011.

[5] C. Cao, M. Weinreb, and H. Xu, "Predicting simultaneous nadir overpasses among polar-orbiting meterological satellites for the intersatellite calibration of radiometers," *J. Atmos. Ocean. Technol.*, vol. 21, no. 4, pp. 537–542, Apr. 2004.

[6] C. Cao, H. Xu, J. Sullivan, L. McMillin, P. Ciren, and Y. Hou, "Intersatellite radiance biases for the High Resolution Infrared Radiation Sounders (HIRS) onboard NOAA-15, -16, and -17 from simultaneous nadir observations," *J. Atmos. Ocean. Technol.*, vol. 22, no. 4, pp. 381–395, 2005.

[7] K. Gopalan, W. Linwood Jones, S. Biswas, S. Bilanow, T. Wilheit, and T. Kasparis, "A time varying radiometric bias correction for the TRMM microwave imager," *IEEE Trans. Geosci. Remote Sens.*, vol. 47, no. 11, pp. 3722–3730, Nov. 2009.

[8] V. John, G. Holl, S. A. Buehler, B. Candy, R. W. Saunders, and D. E. Parker, "Understanding inter-satellite biases of microwave humidity sounders using global SNOs," *J. Geophys. Res.*, vol. 117, p. D02 305, Jan. 2012.

[9] T. Mo, "Calibration of the NOAA AMSU-A radiometers with natural test sites," *IEEE Trans. Geosci. Remote Sens.*, vol. 49, no. 9, pp. 3334–3342, Sep. 2011.

[10] T. C. Connor, M. W. Shephard, V. H. Payne, K. E. Cady-Pereira, S. S. Kulawik, M. Luo, G. Osterman, and M. Lampel, "Long-term stability of TES satellite radiance measurements," *Atmos. Meas. Tech.*, vol. 4, pp. 1723–1749, 2011.

[11] A. J. Geer, P. Bauer, and N. Bormann, "Solar biases in microwave imager observations assimilated at ECMWF," *IEEE Trans. Geosci. Remote Sens.*, vol. 48, no. 6, pp. 2660–2669, Jun. 2010.

[12] G. Ohring, B. Wielicki, R. Spencer, B. Emery, and R. Datla, "Satellite instrument calibration for measuring global climate change," *Bull. Amer. Meteorol. Soc.*, vol. 86, no. 9, pp. 1303–1313, Sep. 2005.

[13] *GCOS-107: Global Climate Observing System (GCOS), Systematic Observation Requirements for Satellite-Based Products for Climate*, Doc. WMO/TD 1338, Sep. 2006.

[14] R. P. Allan, A. Slingo, S. F. Milton, and M. E. Brooks, "Evaluation of the Met Office global forecast model using Geostationary Earth Radiation Budget (GERB) data," *Q. J. R. Meteorol. Soc.*, vol. 133, no. 629, pp. 1993–2010, Oct. 2007.

[15] T. Davies, M. J. P. Cullen, A. J. Malcolm, M. H. Mawson, A. Staniforth, A. A. White, and N. Wood, "A new dynamical core for the Met Office's global and regional modelling of the atmosphere," *Q. J. R. Meteorol. Soc.*, vol. 131, no. 608, pp. 1759–1782, Apr. 2005.

[16] F. Rawlins, S. P. Ballard, K. J. Bovis, A. M. Clayton, D. Li, G. W. Inverarity, A. C. Lorenc, and T. J. Payne, "The Met Office global four-dimensional variational data assimilation scheme," *Q. J. R. Meteorol. Soc.*, vol. 133, pp. 347–362, 2007.

[17] D. Li and K. P. Shine, "A 4-dimensional ozone climatology for UGAMP models," Nat. Environ. Res. Council, Swindon, U.K., UGAMP Internal Rep. 35, 1995.

[18] J. D. Stark, C. J. Donlon, M. J. Martin, and M. E. McCulloch, "OSTIA: An operational, high resolution, real time, global sea surface temperature analysis system," presented at the Proc. IEEE OCEANS Eur., Aberdeen, Scotland, 2007, Paper 061214-029.

[19] R. Saunders, M. Matricardi, and P. Brunel, "An improved fast radiative transfer model for assimilation of satellite radiance observations," *Q. J. R. Meteorol. Soc.*, vol. 125, no. 556, pp. 1407–1426, Apr. 1999.

[20] V. Sherlock, "ISEM-6: Infrared Surface Emissivity Model for RTTOV-6," Met Office, Exeter, U.K., NWP Tech. Rep. 287, 1999.

[21] G. Deblonde and S. J. English, "Evaluation of the FASTEM-2 fast microwave oceanic surface emissivity model," in *Tech. Proc. ITSC-XI Budapest*, Sep. 20–26, 2000, pp. 67–78.

[22] J. Cameron, The effectiveness of the AIRS bias correction of various air-mass predictor combinations, Met Office, Exeter, U.K., NWP Tech. Rep. 421. [Online]. Available: http://www.metoffice.gov.uk/media/pdf/0/9/FRTR421.pdf

[23] N. Atkinson, J. Cameron, B. Candy, and S. J. English, "Bias correction of satellite data at the Met Office," presented at the ECMWF/EUMETSAT NWP-SAF Workshop Bias Estimation Correction Data Assimilation, ECMWF, Bracknell, U.K., Nov. 8–11, 2005. [Online]. Available: http://www.ecmwf.int/publications/library/do/references/list/22022006

[24] J. Hocking, P. N. Francis, and R. W. Saunders, "Cloud detection in Meteosat Second Generation imagery at the Met Office," *Meteorol. Appl.*, vol. 18, no. 3, pp. 307–323, Sep. 2011.

[25] NWP SAF AAPP Documentation: Scientific Description. NWPSAF-MF-UD-001, 2006. [Online]. Available: http://research.metoffice.gov.uk/research/interproj/nwpsaf/aapp/NWPSAF-MF-UD-001_Science.pdf

[26] S. J. English, J. R. Eyre, and J. A. Smith, "A cloud-detection scheme for use with satellite sounding radiances in the context of data assimilation for numerical weather prediction," *Q. J. R. Meteorol. Soc.*, vol. 125, no. 559, pp. 2359–2378, Oct. 1999.

[27] E. G. Pavelin, S. J. English, and J. R. Eyre, "The assimilation of cloud-affected infrared satellite radiances for numerical weather prediction," *Q. J. R. Meteorol. Soc.*, vol. 134, pp. 737–749, 2008.

[28] A. M. Závody, C. T. Mutlow, and D. T. Llewellyn-Jones (2000, May). Cloud clearing over the ocean in the processing of data from the Along-Track Scanning Radiometer (ATSR). *J. Atmos. Ocean. Technol.* [Online]. *17(5)*, pp. 595–615.

[29] A. G. O'Carroll, J. G. Watts, L. A. Horrocks, R. W. Saunders, and N. A. Rayner (2006, May). Validation of the AATSR Meteo product sea surface temperature. *J. Atmos. Ocean. Technol.* [Online]. *23(5)*, pp. 711–726.

[30] C. Merchant, D. Llewellyn-Jones, R. Saunders, N. Rayner, E. Kent, C. Old, D. Berry, A. Birks, T. Blackmore, and G. Corlett, "Deriving a sea surface temperature record suitable for climate change research from the along-track scanning radiometers," *Adv. Space Res.*, vol. 41, no. 1, pp. 1–11, 2008.

[31] X. Liang and A. Ignatov, "Monitoring of IR Clear-Sky Radiances over Oceans for SST (MICROS)," *J. Atmos. Ocean. Technol.*, vol. 28, no. 10, pp. 1228–1242, Oct. 2011.

[32] T. Hewison and J. Mueller, "Ice contamination of Meteosat/SEVIRI implied by inter-calibration against Metop/IASI," *IEEE Trans. Geosci. Remote Sens.*, vol. 51, no. 3, pp. 1182–1186, Mar. 2013.

[33] W. Bell, S. J. English, B. Candy, N. Atkinson, F. Hilton, N. Baker, S. D. Swadley, W. F. Campbell, N. Bormann, G. Kelly, and M. Kazumori, "The assimilation of SSMIS in numerical weather prediction models," *IEEE Trans. Geosci. Remote Sens.*, vol. 46, no. 4, pp. 884–900, Apr. 2008.

[34] D. A. Elliott and H. Aumann, "Sensitivity of AIRS and IASI radiometric calibration to scene temperature," in *Proc. SPIE*, 2011, vol. 8153, pp. 815 303-1–815 303-8.

[35] B. Ingleby, A. Lorenc, K. Ngan, R. Rawlins, and D. Jackson, Improved variational analyses using a nonlinear humidity control variable: Formulation and trials, Met Office, Exeter, U.K., NWP Tech. Rep. 558. [Online]. Available: http://www.metoffice.gov.uk/archive/forecasting-research-technical-report-558

Roger W. Saunders received the Ph.D. degree from Imperial College, University of London, London, U.K., in 1980.

Since then, he has been working in the field of satellite remote sensing with the Met Office, Exeter, U.K., where he heads a group working on the applications of satellite imagery data for numerical weather prediction and forecasting. He was also the Advanced Microwave Sounding Unit-B Instrument Scientist from 1992 to 1995 and the Head of the satellite section with the European Centre for Medium-Range Weather Forecasts from 1995 to 1999. Most recently, he has been leading a group in the European Space Agency to promote the use of satellite data for climate research applications.

Thomas A. Blackmore received the B.Sc. degree in meteorology from the University of Reading, Reading, U.K., in 2005.

Since graduating, he has been with the Satellite Applications Group, Met Office, Exeter, U.K. His research is aimed at improving satellite image data processing, interpretation, and assimilation capabilities at the Met Office for numerical weather prediction and forecasting.

Brett Candy received the B.Sc. degree in physics from Imperial College, University of London, London, U.K., in 1993 and the M.Sc. degree in meteorology from the University of Reading, Reading, U.K., in 2002.

Since 1996, he has been with the Met Office, Exeter, U.K., where he has worked on several applications of remote sensing data for operational numerical weather prediction. He is currently working on a scheme to assimilate satellite observations of soil moisture and surface temperature in order to improve the land surface representation within weather forecasting models.

Peter N. Francis received the D.Phil. degree from the University of Oxford, Oxford, U.K., in 1991.

After graduating, he was with the Meteorological Research Flight Facility, Met Office, Farnborough, U.K., for ten years, where he carried out research into the radiative properties of clouds and aerosols. Since 2001, he has been with the Satellite Applications Group, Met Office, Exeter, U.K., primarily carrying out research into the use of Meteosat Second Generation imagery data for quantifying the physical properties of clouds and volcanic ash.

Tim J. Hewison (M'96–SM'13) received the Ph.D. degree in meteorology, with thesis on the use of ground-based microwave radiometers for atmospheric temperature and humidity profiling, from the University of Reading, Reading, U.K., in 2006.

He is currently a Meteorological Scientist with the European Organisation for the Exploitation of Meteorological Satellites, Darmstadt, Germany, concentrating on the calibration of current, past, and future satellite instruments. He is also currently the Chair of the Research Working Group of the Global Space-based Inter-Calibration System.